Preparation of battery-grade $LiFePO_4$ by the precipitation method: a review of specific features*

A. V. Babkin,[a★] **A. V. Kubarkov,**[a] **E. A. Styuf,**[b] **V. G. Sergeyev,**[a] **O. A. Drozhzhin,**[a] **and E. V. Antipov**[a,b]

[a]*Lomonosov Moscow State University, Department of Chemistry,*
Build. 3, 1 Leninskie Gory, 119991 Moscow, Russian Federation.
E-mail: A.V.Babkin93@yandex.ru
[b]*Skolkovo Institute of Science and Technology, Centre of Energy Science and Technology,*
Build. 1, 30 Bolshoy Boulevard, 121205 Moscow, Russian Federation.
E-mail: inbox@skoltech.ru

The precipitation method is an efficient, economically feasible, and reproducible synthetic route to cathode materials for lithium-ion batteries with attractive performance characteristics, in particular, lithium iron phosphate ($LiFePO_4$). This paper reviews the mechanisms of the key steps of the synthesis, namely, precipitation of iron phosphate $FePO_4$ followed by its sintering with a lithium-containing raw material to give the $LiFePO_4$ phase. The most probable interactions determining the kinetics of the precipitation process are considered using the data on the dissociation degree of the reacting components. The influence of the nature and concentrations of the commonly used sources of iron ($FeSO_4$, $FeCl_3$, $Fe(NO_3)_3$) and phosphorus (H_3PO_4, $NH_4H_2PO_4$, $(NH_4)_2HPO_4$), as well as the precipitation conditions (pH, temperature) on the precipitation efficiency of $FePO_4$ is analyzed. The effect of the nature of the lithium-containing raw material (LiOH, Li_2CO_3, $LiNO_3$) and the sintering (calcination) temperature on the morphology, phase composition, and electrochemical properties of the resulting $LiFePO_4$ is discussed. The possibility is considered of obtaining spherical particles with high bulk density, which provides high specific and volumetric energy density of electrochemical cells. Based on the relationships established, optimal parameters for the synthesis of $LiFePO_4$ with preliminary $FePO_4$ precipitation step are proposed.

Key word: precipitation, iron phosphate, sintering, lithium iron phosphate, synthesis parameters, morphology, electrochemical characteristics.

Introduction

Currently, the rate of industrial development and the growth of global population significantly increase the demand for sustainable energy generation and storage systems.[1] Electrification is becoming a key factor contributing to the intensive development of industry and economy in many countries. One of the main directions in this area is the use of renewable energy sources, which favors significant reduction of the environmental impact and climate change mitigation. The most important renewable energy sources are the Sun, wind, water, and biomass processing products.[2] In spite of their substantial potential, renewable energy is at most 15% of primary energy supply; however, this value is growing every year.[3]

Widespread introduction of stand-alone electricity supply systems is impossible without the development and production of energy storage and transmission devices. A large proportion of renewable energy is accumulated within rather short time intervals associated with periods of maximum solar activity during daylight hours, high and low tides, local increase in wind flow velocity, *etc.* In the cities, the highest energy demand occurs in the morning and evening when the solar activity is far from being maximal. That is why renewable energy received from the sources mentioned above must be efficiently stored for further use. This can be done using battery energy storage systems that can store electrical energy for a long time with minimal losses.[4,5]

---

* Dedicated to Academician of the Russian Academy of Sciences M. P. Egorov on the occasion of his 70th birthday.

Published in Russian in *Izvestiya Akademii Nauk. Seriya Khimicheskaya,* Vol. 73, No. 1, pp. 14—32, January, 2024.

Lithium-ion batteries (LIBs) are the most promising and rapidly developing type of electrical energy storage systems.[1] Currently, there are more than 9 billion mobile devices, laptops, and tablet PC worldwide, most of which use LIBs.[6] In the last decade there has been intensive development of LIBs for use in commercial, municipal, and personal electrical vehicles, as well as for industrial power generation systems.[7] Lithium-ion batteries offer a number of significant advantages over well-known analogues, *viz.*, high operating voltage,[8] high specific energy,[9] long operating life,[10] and a relatively high environmental safety (compared to Ni—Cd or Pb-acid batteries).[11,12] At the same time, in spite of these advantages, the available LIBs have significant drawbacks, such as high cost and safety problems when using cobalt-containing cathode materials.[13—17]

Olivine-type lithium iron phosphate $LiFePO_4$ (LFP) has high thermal stability, thus being much more safe than most other electrode materials and less expensive and toxic than the oxide cathode materials ($LiCoO_2$ and its derivatives). That is why LFP is the most promising cathode material, as was additionally confirmed by LIB market trends in recent years.[18,19] Of course, LFP as the LIB cathode material has some drawbacks including low electronic conductivity,[20] low coefficient of solid-state diffusion of lithium ions,[21] and a relatively low energy density of LFP-based LIBs.[22]

There are many proven methods for efficient reduction of the effects of most these disadvantages on the electrochemical performance of LFP-based cathode materials.[23] For instance, the electron transport in cathode materials is often improved by coating LFP particles with a carbon layer. The conductive carbon layer is formed on the surface of particles of the active material during the sintering with the carbon-containing precursors. This leads to significant increase in the conductivity and capacity of electrodes made of such materials.[24—26]

To intensify solid-state diffusion of lithium ions in the charge—discharge processes, LFP nanoparticles are synthesized. The smaller the particle size of the active material the shorter the diffusion path length of lithium ions to the interface and the actual time taken to extract the same amount of lithium.[27,28] It is important that the volumetric specific energy of the system be conserved. To solve the problem, methods were developed involving the formation of porous secondary micrometer-sized LFP particles representing agglomerated nanocrystallites.[29] The secondary particles can be of different size, which allows particles of smaller diameter to fill voids between particles of larger diameter and thus to increase the packing density of the LFP particles in the electrode and, as a consequence, the specific energy of the entire system.[30]

Thus, at present many problems of LFP-based electrochemical systems already have effective practical solutions.[31,32] The remaining challenges include the choice of the method for the synthesis of LFP and optimization of parameters aimed at preparing active material particles of specified shape and size.[33]

The commonly used methods for the synthesis of LFP particles can be divided into solid-phase and liquid-phase ones.[34—36] The first group includes mechanochemical activation, carbothermal reduction, microwave heating, solid-phase synthesis, *etc*. The second group includes hydro- and solvothermal synthesis, sol—gel technique, lyophilization, precipitation, *etc*.

All these methods have their own advantages and drawbacks. Solid-phase synthesis is technologically simple to implement in industrial conditions; however, it often requires rather high temperatures. The active material particles thus obtained are heterogeneous in composition and have low electrochemical performance, especially, at high current densities. Since the process takes a long time, the energy consumption for its implementation is rather high, while multiple grinding and calcination can lead to formation of larger aggregates.[36] Mechanochemical activation allows one to obtain small structurally uniform particles with larger specific surface area and, as a consequence, higher reactivity. However, the method is energy-consuming and the synthesized particles can contain impurities that are formed during intense contact with grinding bodies (this is also characteristic of solid-phase synthesis). In addition, long-term high-rate milling can lead to local overheating of particles and subsequent decomposition of the precursors without formation of the target product.[36,37] Microwave heating enables rapid and efficient synthesis of particles of different shape and size, which considerably reduces the duration of the process and the amount of energy required. However, the method provides nonuniform heating of the sample structure, which leads to incomplete interaction between the components and to formation of stable intermediate products and impurities. Practical implementation of the approach requires expensive equipment. Besides, in this case it is difficult to maintain simultaneous mechanical mixing and the course of the process cannot be controlled from the outside.[38]

Liquid-phase methods for the synthesis also have significant drawbacks; however, they are simpler to implement compared to the solid-phase approaches. Hydrothermal synthesis is most widely used in the laboratory conditions. It is quite simple to implement, not energy-consuming, and does not require complex equipment. Its major drawback is a large number of parameters to control in order to ensure the reproducibility of the properties of the target materials.[38,39] In addition, the vapor pressure developed in the reactor during the synthesis imposes limitations on the volume of the apparatuses. The sol—gel method is complicated by the long duration of the process and by the formation of a large amount of side products during the calcination step.[38] The most promising methods include spray drying and spray pyrolysis which enable rapid and inexpensive preparation of micrometer-sized spherical particles of the active material in a short time. The main drawback of these methods consists in complex process equipment, which undoubtedly increases the final cost of the product.[35] Eventually, the precipitation method of $FePO_4$ followed by sintering of the precursor with the lithium source uses available and inexpensive raw materials and enables rapid and reproducible preparation of particles of the active material with the desired morphology. The process does not require high temperatures or long-term treatment at elevated pressures; however, it is of paramount importance to strictly control the medium pH and temperature.

Among the above methods for the synthesis of LFP, the approach involving precipitation of $FePO_4$ as a preliminary step is most appropriate for reproducible preparation of LFP particles of specified shape and size for high-performance LIB applications.[40] Note that precipitation is a key step in the synthesis of spherical lithium iron phosphate particles (Fig. 1). Iron phosphate obtained in the first step by the precipitation method is then sintered with the lithium-containing raw material and the carbon-containing precursor to obtain spherical particles coated with conductive carbon layer.

The currently available literature data on the effect of various parameters of the synthesis of LFP by the preliminary precipitation of iron phosphate on the

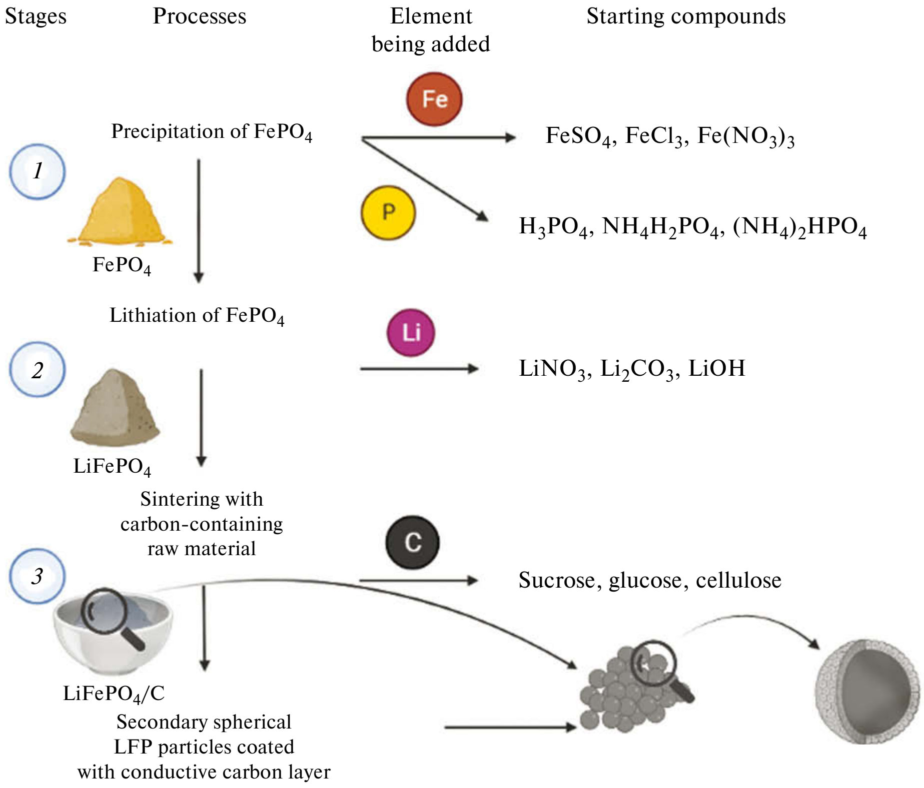

Fig. 1. Synthesis of lithium iron phosphate (LFP) by the precipitation method: main stages.

electrochemical characteristics of the material are fragmentary. Clearly, the nature of the raw material and the main synthesis parameters (pH value, temperature, process duration) should strongly influence the properties of the synthesized active materials.[41—43]

In this review we attempt to summarize the published experimental data on the specific features of the synthesis of LFP particles by the precipitation method and to demonstrate how the parameters of the precipitation process and subsequent sintering influence the phase composition, morphology, and electrochemical properties of the synthesized materials.

Precipitation of $FePO_4$ using different raw materials: specific features

Precipitation processes are widely used in industry and methods for their implementation are well known. Precipitation techniques are used in hydrometallurgy,[44] sublimational separation technique,[45] analytical chemistry, and radiochemistry for concentration of target components.[46] The precipitation methods, as well as adsorption techniques allow one to identify components with very low limits of detection — 10^{-8}—10^{-10} wt.%.[47] Metal phosphating by precipitation is used in, *e.g.*, automotive industry.[48]

The wide use of precipitation methods suggests the possibility of predictable control of the process and the preparation of materials with high reproducibility of their physicochemical properties. The classical precipitation process represents the transition of macrocomponents from a saturated solution simultaneously containing various compounds to a precipitate. The solution obtained by mixing two solutions of specified concentrations appears to be supersaturated with respect to iron phosphate, which forms a precipitate. In most cases the efficiency of the precipitation process depends strongly on its duration, temperature, medium pH, and on the concentrations of the starting reagents (Fig. 2).

Presumably, the main precipitation mechanisms of $FePO_4$ involve fluctuational formation in the metastable phase, which induces nucleation of the new phase (seeds of a certain size), as well as electrostatic interaction between oppositely charged iron cations and phosphoric acid anions (nucleation) accompanied by a decrease in the Gibbs free energy. As a result, the primary amorphous structure of the precipitate is formed. Then, ions from the solution can adsorb on the energetically inhomogeneous

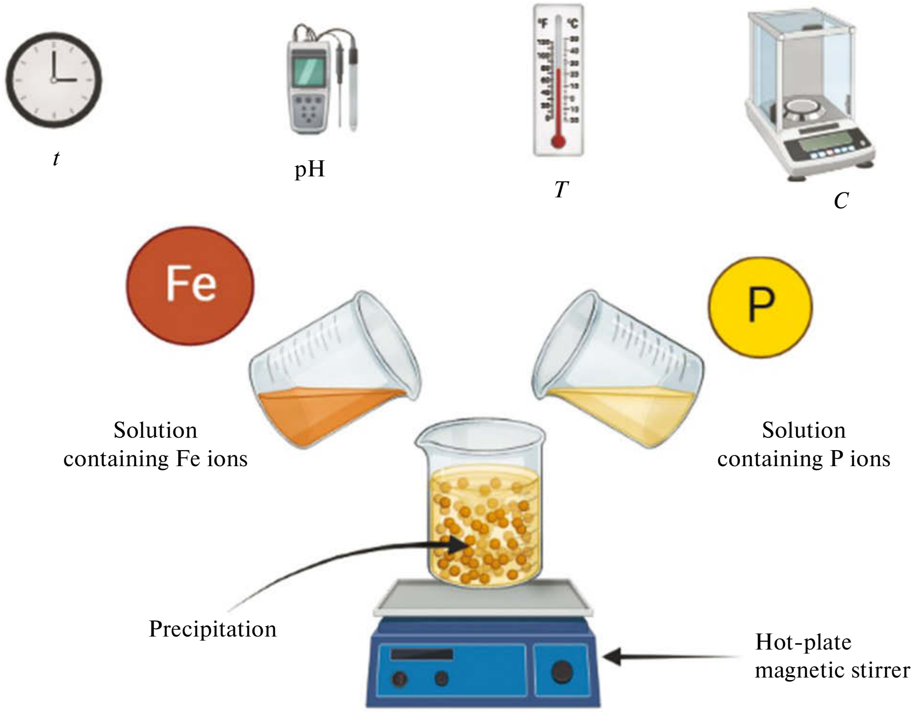

Fig. 2. Synthesis of iron phosphate $FePO_4$ by the precipitation method.

surface of the particles being formed, thus initiating their further growth. Ions are mainly adsorbed on the surface defects of the amorphous aggregates, which favors a decrease in the free energy of the system. As the particle size increases, the solid—solution interface extends and, as a consequence, the precipitation rate increases. To continue the precipitation process, the concentrations of the dissolved substances should be higher than the saturation concentration.

The most often used iron-containing reagents for the synthesis of $LiFePO_4$ by the precipitation method include $Fe(NO_3)_3 \cdot 9H_2O$,[49] $FeCl_3$,[50] $FeSO_4 \cdot 7H_2O$,[51] and $FeC_2O_4 \cdot 2H_2O$.[52] Among them, iron chloride and iron sulfate are inexpensive and readily available.[53,54] All these salts undergo multistep dissociation and hydrolysis in neutral solutions. The formation of isolated trivalent iron cations in weakly acidic and neutral media (pH ~5—7) is hardly probable because free cations interact with the hydroxide anions that are formed upon dissociation of water molecules to give insoluble forms of iron hydroxides.

To suppress the side processes of formation of insoluble iron hydroxides, the iron phosphate precipitation is performed in strongly acidic media (usually, at $\text{pH} \leqslant 3$). Note that the concentrations of the starting reagents and the precipitation temperature can also in different manner suppress the formation of insoluble forms of iron hydroxides. For instance, almost no $Fe(OH)_3$ is formed at an initial concentration of Fe^{3+} ions of about 0.1 mol L^{-1} at $\text{pH} < 2$. When using divalent iron compounds (*e.g.*, $FeSO_4$), hydrogen peroxide H_2O_2 can be utilized as an auxiliary reagent to increase the oxidation state of iron.[55]

In most cases, including the precipitation technique, $LiFePO_4$ is synthesized using orthophosphoric acid, ammonium hydrophosphate or ammonium dihydrophosphate as the phosphorus-containing raw materials.[56] Dissociation of H_3PO_4 in aqueous solutions is characterized by the preferred formation of $H_2PO_4^-$ ions ($K_{a1} = 7.24 \cdot 10^{-3}$)[57] whose concentration is about 10^5 times higher than that of the doubly charged ions HPO_4^{2-} formed in the second step of dissociation ($K_{a2} = 6.2431 \cdot 10^{-8}$). It should be noted that only the first step of dissociation is an exothermic process. Since the formation constant of free phosphate anions PO_4^{3-} is low ($K_{a3} = 4.8 \cdot 10^{-13}$), their concentration can be neglected.

Taking account of possible hydrolysis and dissociation of the starting reagents and having combined the reactions,[57—61] one can assume that the precipitation process involves multistep formation of nanoparticles of different composition. Usually, the overall process affords particles of mixed composition and structure having arbitrary shape and size. Almost all intermediate products are formed with elimination of excess protons, which increases the medium acidity.

It should be noted that the average particle size and the structure of $FePO_4$ can depend strongly on the parameters of the precipitation process (concentration, temperature, medium pH, *etc.*).

Precipitation conditions and their effect on the properties of $FePO_4$

Effect of the initial concentrations of iron and phosphorus ions. Ferric phosphate particles can form in a wide range of initial reactant concentrations. It was shown[62] that changes in the concentrations of iron(II) cations and phosphate anions (at 1 : 1 molar ratio of the components) influence the size of $FePO_4$ particles and thus determines their electrochemical performance in the charge—discharge processes. An increase in the concentration of Fe^{2+} ions in the starting solution from 0.1 to 0.4 mol L^{-1} was followed by the formation of smaller particles (400×250 *vs.* 200×100 nm, respectively). As the concentration of the starting reagents increases, the number of nucleation sites appeared in the course of electrostatic interaction between ions in the solution increases dramatically. The higher the charge of the cation the stronger its adsorption on a crystal nucleus.[63] The reaction was accompanied by intense nucleation and subsequent growth of crystallites. An increase in the concentration of the Fe-containing raw material naturally led to an increase in the concentration of nucleation sites and the frequency of collisions between a particular nucleus and dissociated ions decreased. As a result, the particle growth rate and the size of the particles being precipitated also decreased.

Similar results were obtained using $Fe(NO_3)_3$ and $(NH_4)_2HPO_4$ as the starting reagents, other things being equal.[64] Precipitation from the solution with a $Fe(NO_3)_3$ concentration of 0.1 mol L^{-1} afforded large $FePO_4$ particles with a broad particle size distribution from about 2 to nearly 25 μm. Uniform

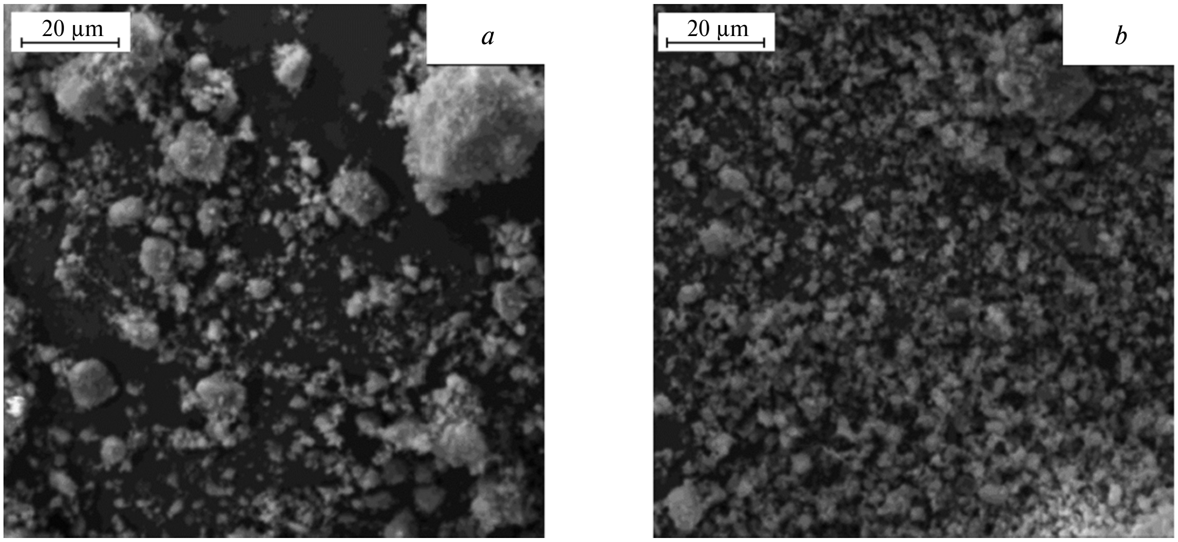

Fig. 3. Photomicrographs of $FePO_4$ nanoparticles prepared by the precipitation method from solutions with initial concentrations of 0.1 (*a*) and 1 mol L^{-1} (*b*).[64]

particles with the sizes from nearly 2 to 10 μm formed from the solution with a concentration of 1 mol L^{-1}. Scanning electron microscopy studies showed that the precipitated particles had arbitrary shapes and rough surfaces irrespective of the concentration of the starting substrates (Fig. 3).

It follows that the average size of the $FePO_4$ particles being precipitated can be varied by varying the concentrations of the starting reagents. At high concentration, a larger amount of smaller uniform particles is produced. As the concentration decreases, the number of nuclei decreases and, as a consequence, a smaller number of larger particles is formed because the probability of their interaction with ions in the solution increases.

Effect of the solution pH. The precipitation efficiency of $FePO_4$ is influenced by the solution pH, other things being equal.[65] An analysis of possible reactions showed that the solution pH influences the character of the interaction between the reagents and specifies the nature of reaction products. A thermodynamic boundary of the solution pH was determined, which specifies the composition of the precipitated ions.[66] At pH 1.72, hydrated $FePO_4$ precipitates, while simultaneous precipitation of iron phosphate and iron hydroxides begins at pH 1.72. It was established that in the pH value range of 1.72—4 the concentration of Fe^{3+} ions in the solution continues to decrease, while the concentration of dissolved phosphate complexes ($HPO_4{}^{2-}$) increases, thus being indicative of the formation of side reaction products. A thorough study[65] of the optimum range of pH values (from 0.4 to 1.72) was aimed at determining the pH value corresponding to the maximum efficiency of the precipitation process at specified initial concentrations of the iron- and phosphorus-containing raw materials (0.4—0.5 mol L^{-1}). It was established that the optimum range of pH values for the synthesis of $FePO_4$ is from 0.4 to 0.8. Subsequent increase in the solution pH does not improve the precipitate yield and even to some extent worsens it. For instance, the X-ray diffraction patterns of the precipitates obtained at pH 0.9 and 1.0 revealed the presence of compounds identified as the $(NH_4)Fe_2(PO_4)_2(OH) \cdot 2H_2O$ phase. Thus, the optimum solution pH value for the precipitation process is about 0.8.Precipitation of iron phosphate from processed laterite residue was analyzed[57] using thermodynamic calculations. It was demonstrated that the operating window corresponding to stable formation of solid $FePO_4 \cdot 2H_2O$ matches region A (Fig. 4), whereas region B (initial concentration of orthophosphoric acid was 6 mol L^{-1}) corresponds to efficient leaching of iron from the iron-containing raw material. Therefore, stable precipitation of the iron phosphate phase containing no iron hydroxide impurity requires that the medium pH value be maintained in region A. This conclusion is confirmed by

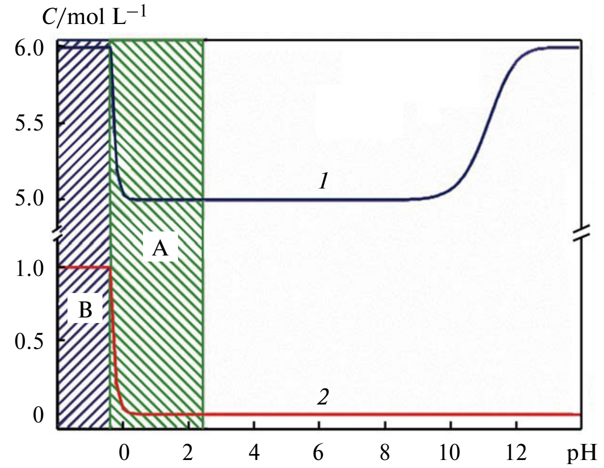

Fig. 4. The pH range corresponding to stable formation of the $FePO_4 \cdot 2H_2O$ phase[57]: [P] (*1*) and [Fe] (*2*); for the regions A and B, see text.

the results obtained in another study,[67] where precipitation of iron hydroxides began at similar upper-bound pH values.

It was also reported[68] that the solution pH can influence the size of particles being precipitated. At pH 1, larger aggregates 1.5—2 μm in size are formed, while a further increase in the solution pH to a value of 2 to 3 favors the formation of smaller spherical particles 200—350 nm in size. This is probably due to specific features of the dissociation of phosphate complexes. At low pH values, mainly the first step of dissociation of the acid proceeds owing to high concentration of protons, while the iron ions are present in the solution in the form of Fe^{3+}cations (hydrolysis can be neglected in this range of pH values). It follows that an iron cation can simultaneously interact with three $H_2PO_4^-$ anions.

As the solution pH increases, the dissociation of phosphoric acid proceeds more efficiently, which favors an increase in the concentration of the dissociated anions and, as a consequence, nuclei. As a result, the size of the precipitated particles decreases.

The effect of the ζ-potential of the surface of the particles being precipitated on the precipitation efficiency should also be mentioned. It was reported[69] that the isoelectric point of $FePO_4$ is at pH ~3.9. At pH < 3.9, particles have a positively charged surface, while at pH > 3.9, the surface bears a negative charge. The actual surface charge can make the Coulomb interaction in the course of precipitation less efficient (iron cations Fe^{3+} will repel from the positively charged particle surface). Therefore, the closer the solution pH value to the isoelectric point the more efficient the precipitation process. However, the formation of side products, *viz.*, iron hydroxides is possible at pH 2—3 (see above).

Thus, the range of formation of solid hydrated $FePO_4$ can be extended by increasing the acid concentration. In the strongly acidic media, the process is limited to retarded dissociation of phosphoric acid, while at pH ~ 3 it is limited by the formation of insoluble forms of iron hydroxides. Based on the results of our analysis, the highest precipitation efficiency can be achieved in the pH range from 0.3 to 2.6 at initial concentrations of the iron and phosphorus ions in the range from ~0.5 to ~1.5 mol L^{-1}.

Effect of the solution temperature and the precipitation duration. The solution temperature has strong effect on the kinetics and phase composition of reaction products synthesized by the precipitation method.[70,71] The higher the temperature the higher the entropy of the process.[72] Besides, the higher the internal energy of the system the larger the displacements of the ions or molecules brought into contact from their equilibrium positions; this favors destabilization of the entire system and leads to more efficient dissociation and subsequent interaction.[73]

Studies of the $FePO_4$ precipitation from aqueous solutions revealed that the structure and size of aggregates being formed depend strongly on the solution temperature. The effects of the reaction time and solution temperature on the size of iron phosphate particles are illustrated in Fig. 5.[74]

It was established that heating from 15 to 80 °C favors an increase in the average particle size from about 1 to nearly 8 μm at a process duration of 8 h. Raising the temperature makes the ion—ion contacts more probable, which leads to an increase in the size of particles being formed and in the rate of their agglomeration. As a result, the average size of precipitated particles increases. It seems also probable that the effects of the parameters studied on the size of precipitate particles can depend on the nature of the starting reagents.

Changes in the free energy, Δ*G*, of the system corresponding to the following feasible reaction between iron phosphate and H_3PO_4:

$$FePO_4\downarrow + 2\,H_3PO_4 \longrightarrow Fe^{3+} + 3\,H_2PO_4^-$$

were studied[75] for different temperatures using thermodynamic calculations.

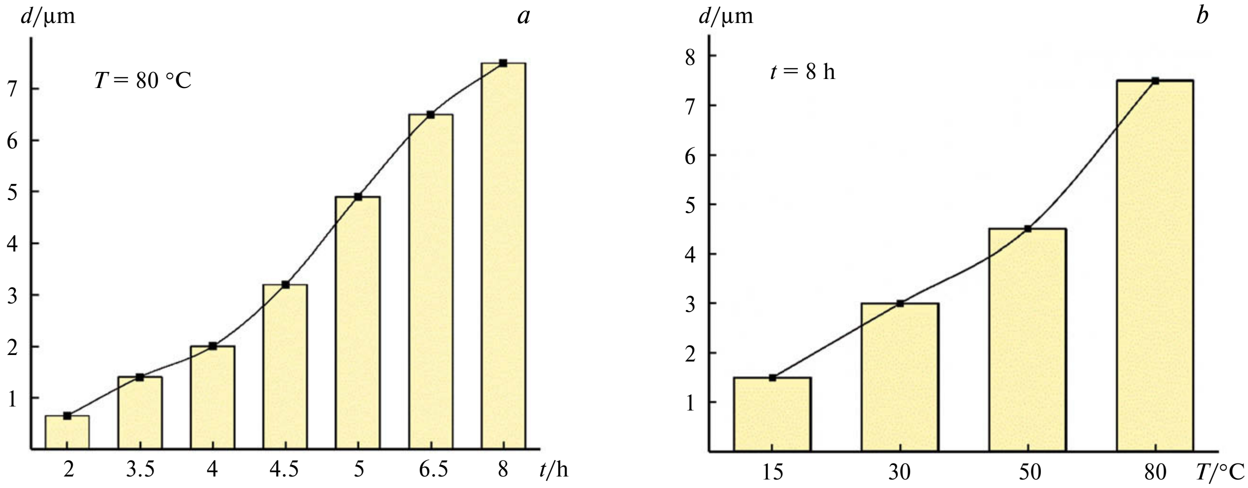

Fig. 5. Effects of reaction time (*a*) and solution temperature (*b*) on the $FePO_4$ particle size.[74]

In the temperature range from 0 to 45 °C the ΔG value is negative. It follows that the reaction is thermodynamically feasible and the precipitated $FePO_4$ can be dissolved in phosphoric acid solutions. At $T > 60$ °C, the ΔG values are positive and, therefore, the reaction in question is impossible.

Similar data on the effect of temperature on the solubility of $FePO_4$ were also reported elsewhere.[57] At 30 °C, the concentration of iron cations in the phosphoric acid solutions is about 10 times higher than at 80 °C, other things being equal. Thus, the extent of the precipitation reaction also increases with increasing solution temperature. It was shown[61] that the precipitation efficiency of iron and phosphorus ions is nearly 100% at a solution temperature of about 95 °C (Fig. 6). This additionally confirms that intensification of precipitation processes requires that the solutions be heated to $T = 80$—100 °C. The solution temperature has strong effect on the iron phosphate solubility which decreases while the precipitation efficiency increases with increasing *T*.[76]

An analysis of the effect of temperature on the stepwise dissociation of phosphoric acid was reported.[77] As shown above, the first step of dissociation is an exothermic reaction. From the standpoint of precipitation processes the more preferable phosphoric acid anions are formed in the second and third steps of dissociation. Raising the temperature causes the exponents of the pK_{a2} and pK_{a3} dissociation constants of phosphoric acid to decrease (*i.e.*, the dissociation constants thus increase), which leads to an increase in the proportion of the HPO_4^{2-} and PO_4^{3-} anions formed in the second and third steps of dissociation, respectively. The increase in the concentrations of the necessary ions will favor a decrease in the concentration of unstable soluble complexes and an increase in the yield of the target reaction product.

Therefore, the temperature of the precipitation process influences not only the iron phosphate precipitation efficiency, but also the morphology of the particles being precipitated and the degree of their crystallinity. The solubility of $FePO_4$ in phosphoric acid solutions decreases considerably with increasing temperature. As a consequence, both the rate of the precipitation process and the yield of the target product increase. In addition, an increase in the solution temperature causes acceleration of the second and third steps of phosphoric acid dissociation and the appearance of the target anions necessary to form insoluble iron(III) complexes.

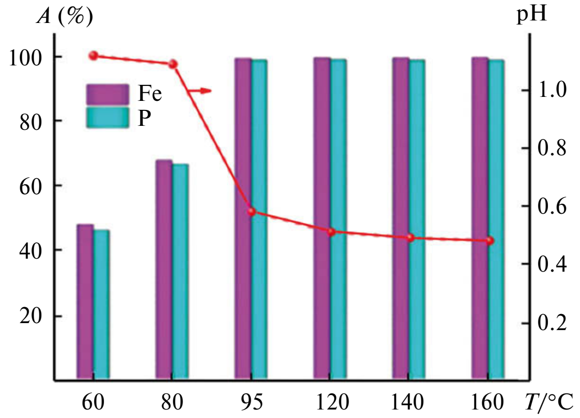

Fig. 6. The precipitation efficiency (*A*) of $FePO_4$ and the pH value after precipitation at different temperatures.[61]

Thus, based on the results obtained, one can formulate some criteria that determine how certain parameters of the precipitation process affect the morphology and structure of the resulting $FePO_4$ particles. Rigorously meeting these criteria, iron phosphate $FePO_4$ can be obtained by the precipitation method with the highest efficiency.

Since the formation of iron phosphate is a multistep process, the interaction of phosphoric acid anions with iron cations in aqueous solutions most probably results in unstable intermediate products. The formation of the target components will be limited by the dissociation constants of the corresponding processes. The size of the resulting particles can be controlled by varying the reagent concentrations. In particular, an increase in the concentration causes the formation of smaller particles owing to an increase in the proportion of nuclei, whereas a decrease in the concentration favors the formation of larger aggregates.

The solution pH value is a key parameter influencing the precipitation efficiency of iron phosphate. In the strongly acidic region, hydrolysis can be suppressed almost completely; however, in this case the degree of the second and third steps of phosphoric acid dissociation are also negligible. The most favorable range of pH values is from 0.3 to 2.6. At higher pH values, insoluble iron hydroxides are formed.

As temperature increases, the iron phosphate solubility decreases considerably and the second and third steps of the dissociation of phosphoric acid as well as the ion—ion contacts with the formation of the target product become much more probable. The maximum efficiency of the process is achieved at solution temperatures in the range from 80 to 95 °C.

Synthesis of $LiFePO_4$ from precipitated $FePO_4$ precursor: specific features

Effect of the nature of the lithium-containing raw material. Iron phosphate obtained by the precipitation method can be used to synthesize the LIB cathode material, $LiFePO_4$.

As mentioned above, the synthesis of LFP using iron phosphate as precursor implies mixing of $FePO_4$ with the lithium-containing raw material followed by sintering under different conditions (see Fig. 1). Note that the structure and morphology of the resulting LFP particles are strongly influenced by the concentrations of the starting reagents, the temperature, the nature of the lithium- and carbon-containing raw materials, *etc.*[78—87] It is important to understand how the synthesis conditions chosen can influence the operating performance of the synthesized cathode material.[88]

The mechanism of formation of LFP particles during sintering involves reduction of iron in $FePO_4$ to Fe^{2+} accompanied by simultaneous embedding of the charge-compensating Li^+ ions into the $LiFePO_4$ lattice being formed. The commonly used lithium-containing raw materials include Li_2CO_3,[89] LiOH,[90] LiOAc,[91] $LiNO_3$,[92] *etc.*

The necessary components are mixed in aqueous or anhydrous media using grinding in a mortar or milling in ball, ring, bead, vibratory, or jet mills to obtain fine and superfine powders with a particle size of 40—100 μm and 40 μm, respectively. Jet mills are more efficient than vibratory or ball mills in obtaining particles 1—5 μm in size. It should be noted that, irrespective of the medium, deviation from stoichiometry when mixing the starting reagents can lead to formation of impurity products by the following feasible reactions:

$$3\,LiOH + FePO_4 \xrightarrow{H_2O} Li_3PO_4 + Fe(OH)_3\downarrow,$$

$$2\,Fe(OH)_3 \xrightarrow{t} Fe_2O_3 + 3\,H_2O.$$

The formation of impurity products can induce the formation of side crystalline phases, which negatively affects the capacity of the resulting composite material. A comparison of the efficiency of LFP/C composites prepared from different lithium-containing raw materials in aqueous and anhydrous conditions was reported.[93] The highest discharge capacity (Q_{disch}) values were obtained for the materials synthesized from LiOH (161 mA h g^{-1}), Li_2CO_3 (155 mA h g^{-1}), and $LiNO_3$ (138 mA h g^{-1}) in anhydrous media. Probably, this is due to the size and morphology of the resulting particles, as well as to nonuniformity of the carbon coating formed on the surface of the active material particles.

An electrochemical performance study[94] of LFP/C composite materials synthesized by the sol—gel method using different lithium-containing sources under identical process conditions gave the following results. The highest discharge capacity was obtained for the composite electrode materials synthesized using LiOH (147.5 mA h g^{-1} at a current density of 0.2 C), Li_2CO_3 (124.1 mA h g^{-1}), and $LiNO_3$ (108.2 mA h g^{-1}). The electrochemical cell with the cathode material synthesized using LiOH had the lowest charge-transfer resistance. This fact was associated with the higher degree of crystallinity of LFP obtained using LiOH, which made it possible to increase the conductivity and ionic mobility, thus decreasing the resistance of the entire system.

The results obtained in another study[95] confirmed that LiOH is the optimum lithium-containing source, which provides the highest electrochemical performance of the LFP material. It is LiOH that allows one to synthesize single-phase LFP and to obtain smaller particles. These factors can be a consequence of higher solubility and higher basicity of lithium hydroxide compared to lithium carbonate (Li_2CO_3) or lithium nitrate ($LiNO_3$). It should be emphasized that high thermal stability of LiOH and Li_2CO_3 in the temperature range to about 700 °C makes them the most efficient Li sources for solid-phase synthesis of $LiFePO_4$, because lithium acetate or lithium nitrate decompose at much lower temperatures (~500 °C).[96] Besides, low-temperature decomposition of lithium nitrate in the course of heating can be accompanied by the release of oxygen-containing compounds that suppress the Fe^{3+}/Fe^{2+} reduction and form impurity phases on the surface of particles, which increases the resistance of the synthesized material.

Currently, there are proven strategies that combine various methods for synthesis and thus allow one to obtain high-performance materials from almost all types of lithium-containing raw materials.[97] This makes it possible to nearly completely exclude the effect of the nature of the raw materials on the morphology and electrochemical performance of the resulting LFP. However, the choice of the key parameters of synthesis and the specific features of formation of a stable carbon coating during sintering still remain open questions.

Effect of the sintering temperature of Fe_3O with the lithium-containing raw material on the electrochemical performance of cathode materials. As mentioned above, sintering of precursors is accompanied by the formation of the LFP crystal structure. The most efficient and widely used method involves sintering with the carbon source (usually, a readily available product of natural origin).[98] High-temperature decomposition of the carbon-containing raw material is followed by the formation of a carbon coating on the surface of synthesized LFP particles[99] that helps solve at least two severe problems related to practical application of the material in the LIB cathodes. First, this allows one to inhibit the growth of particles of the active material during the synthesis (that is, the diffusion path of Li^+ ions is shortened and, as a consequence, a larger amount of the active material becomes involved in the intercalation/deintercalation process).[100] Second, the conductivity and some other electronic properties are improved significantly.[101] For instance, the formation of a carbon coating on the surface of $LiFePO_4$ particles was followed by an increase in the LFP conductivity by about four orders of magnitude.[102] Similar data were obtained in a study of the properties of LFP coated with carbon from different sources, *viz.*, the conductivity of LFP particles increased by 5—6 orders of magnitude.[103]

The heat-treatment temperature, at which amorphous $FePO_4$ is sintered with the lithium and carbon sources to give crystalline $LiFePO_4$, has strong impact on the performance of LFP as the cathode material.

The effect of the calcination temperature in the range of 550—700 °C on the electrochemical performance of $LiFePO_4$ was analyzed.[104] It was demonstrated that at 600 °C and above the crystal structure of the resulting material remains unchanged; however, as the temperature increased to 650 °C, more homogeneous particles were prepared, each being coated with an amorphous carbon layer. At 700 °C, agglomeration of small particles of the active material was observed. The material synthesized at 650 °C had the highest discharge capacity. Similar results were obtained in another study[105] where the material synthesized at 650 °C also demonstrated the highest specific discharge capacity (156.7 mA h g^{-1}) and the best capacity retention after 50 charge—discharge cycles, namely, 96.5% at a current density of 1C (Fig. 7).

This fact was explained by the high electronic conductivity of the cathode material. Indeed, since each $LiFePO_4$ particle is connected to the conductive carbon network, the active material can be fully utilized to achieve high specific capacity and long-term cycling performance.

The effect of the synthesis temperature on the properties of $LiFePO_4/C$ composites was studied[106] in the range from 550 to 750 °C with an increment of 50 °C. The results obtained were much like those

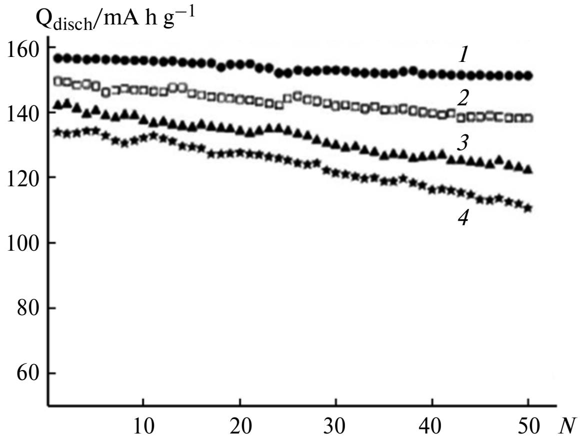

Fig. 7. The cycle performance of LFP/C samples sintered at different temperatures: 650 (*1*), 700 (*2*), 750 (*3*), and 800 °C (*4*).[105]

considered above. The materials prepared at 550 and 600 °C were characterized by very small particle size and low discharge capacity. The latter was attributed to the low degree of crystallinity and low conductivity of the composites in question. At 700 and 750 °C, agglomeration of small particles was observed. As a consequence, the diffusion path of lithium ions in the particles increased and the electrochemical performance of the materials decreased. It follows that the material synthesized at 650 °C has the best electrochemical performance.

The effect of the sintering temperature and the nature of precursors on the electrochemical performance of LFP is illustrated by the data presented in Table 1.

Note that these experimental data allow one to quite reliably determine the temperature range for sintering iron phosphate with the lithium source.

Precipitation as an intermediate step in the synthesis of spherical LFP particles with high bulk density

The most important characteristics of a LIB include the specific discharge capacity normalized to the unit mas of the active material and the specific energy density normalized to the unit volume of the cathode material. Besides, the smaller the particle size of the active material (including the nano size region) the shorter the diffusion path of lithium ions in the charge—discharge processes. However, smaller particles have a much larger specific surface area, which naturally leads to an increase in the electrolyte/electrode contact area and can promote reduction of the electrochemical stability in the charge—discharge processes.[112]

There is a correlation between the morphology of particles of the active material and the volumetric energy density of a LIB.[113] Powders consisting of spherical particles of the active material have a higher packing density than powders consisting of particles of irregular shape. Compared to particles of irregular structure, spherical particles have the smallest free surface area, which decreases the contribution of surface interaction when contacting the electrolyte and the degree of formation of side products that precipitate in the course of electrochemical reaction.

Similar results were also reported in another study.[114] It was demonstrated that, among particles of different morphology, it is spherical particles that have the highest bulk density, which is of particular importance from the standpoint of the volumetric energy density of the electrochemical system. Particles of irregular shape can agglomerate and come

Table 1. Effect of the starting reagents and sintering temperature on the specific discharge capacity of $LiFePO_4$

Raw material	Carbon source	Temperature range/°C	T_{opt}	Maximum discharge capacity/mA h g^{-1}	Reference
$(NH_4)H_2PO_4$, LiOAc, $Fe(OAc)_2$	Sucrose, glucose, acetylene black	550—700	650	155.0	98
$FePO_4 \cdot 2H_2O$, $LiOH \cdot H_2O$	Poly(ethylene glycol)	550—700	650	153.4	104
$FeC_2O_4 \cdot 2H_2O$, LiF, $(NH_4)_2HPO_4$	Carbon gel	650—800	650	156.7	105
$FePO_4$, Li_2CO_3	Glucose	550—750	650	151.2	106
$LiOAc \cdot 2H_2O$, H_3PO_4, $FeCl_2 \cdot 4H_2O$	Citric acid	600—750	650	166.0	107
Li_2CO_3, $(NH_4)H_2PO_4$, Spent $LiFePO_4$	Sucrose	600—750	650	147.1	108
H_3PO_4, LiOH, $FeSO_4 \cdot 7H_2O$	Glucose	600—700	650	154.8	109
Li_2CO_3, $(NH_4)H_2PO_4$, $FeC_2O_4 \cdot 2H_2O$	Pyrene	600—700	650	152.0	110
$FeC_2O_4 \cdot 2H_2O$, $(NH_4)H_2PO_4$, Li_2CO_3	Glucose	600—700	650	163.8	111

* T_{opt} is the optimum sintering (calcination) temperature.

into close contact with one another. Such contacts along a certain crystal face can lead to the formation of excess space surrounding the agglomerates.[115] Owing to their shape, spherical particles have a smaller particle-particle contact area, which improves their wettability. In addition, the total void volume in packings of spherical particles is much smaller, therefore, these particles have a higher bulk density.

It should also be noted that the structure of the carbon coating of particles of irregular shape can be nonuniform, especially, at ends and narrow faces, and can be damaged mechanically or frictionally. The surface of spherical particles is free from these features and thus makes it possible to form a stable and uniform carbon coating.

Among particles of different morphology, it is spherical particles that are optimum from the standpoint of packing density.[116] To additionally increase the bulk density, it is appropriate to use secondary micrometer-sized spherical particles formed by agglomeration of smaller primary particles. Smooth surface of the secondary particles additionally reduces friction and favors the formation of a dense structure when shaking. As a result, it is possible to attain a uniform distribution of particles, their accessibility to wetting with electrolyte, and small surface area.

Spherical particles are prepared by different methods including solid-phase synthesis of LFP.[117] Particles coated with a conductive carbon layer (weight fraction 1.7%) had a rather low bulk density of 1.11 g cm^{-3}. Spherical LFP particles with a bulk density of 1.16 g cm^{-3} were obtained by hydrothermal synthesis.[118] Combining mechanochemical synthesis, spray drying, and carbothermal reduction allowed one to synthesize spherical particles with a bulk density of 1.6 g cm^{-3} (Fig. 8).[119]

Thus, cathode materials consisting of spherical particles of different size will have the highest bulk

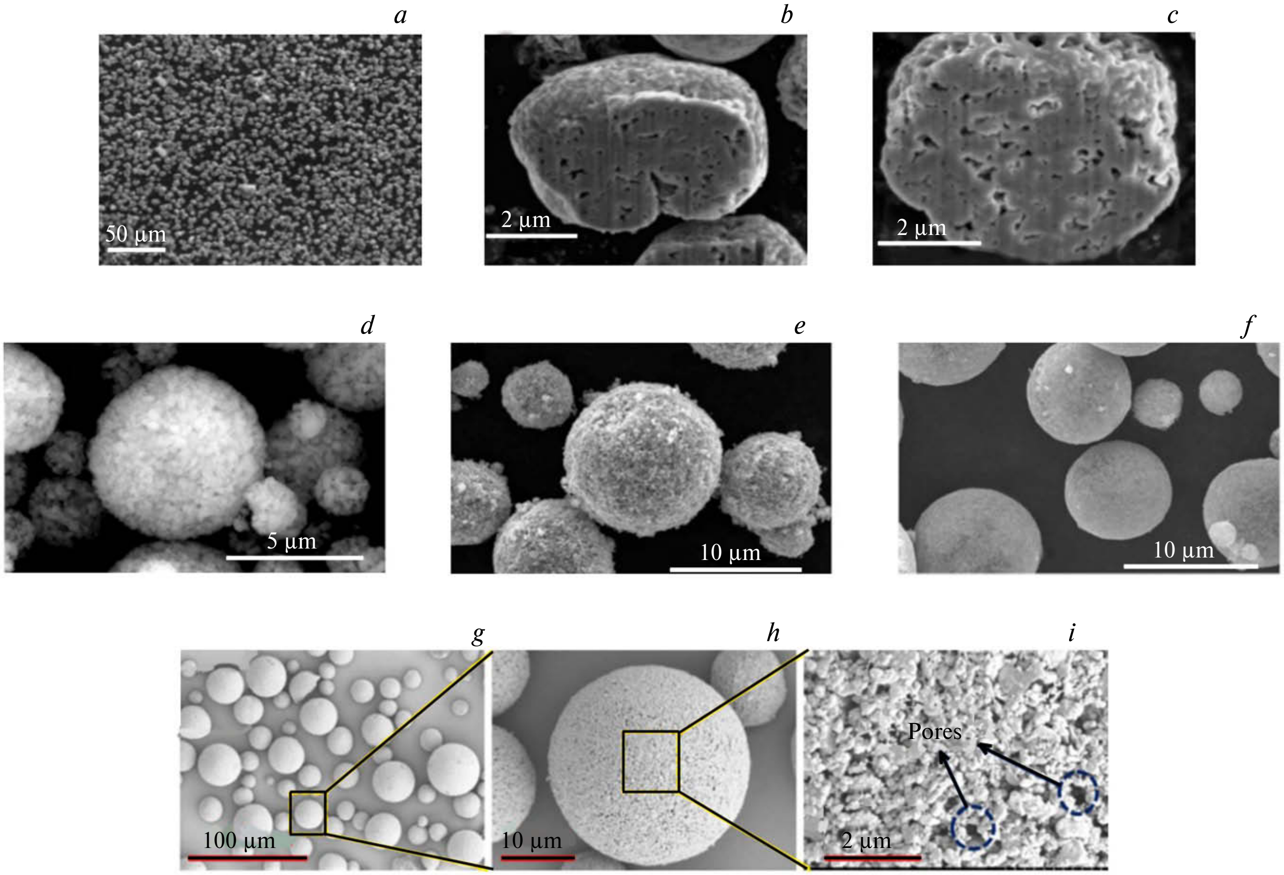

Fig. 8. Photomicrographs of spherical LFP particles obtained by the precipitation method (*a*—*c*),[112] by combining mechanochemical synthesis, spray drying, and carbothermal reduction (*d*—*f*),[119] and by solid-phase synthesis (*g*).[117] *a* —$FePO_4$ precursor at low magnification, *b* and *c* — general view and cross-section of LFP particle, respectively; *d* — spherical LFP particle after spray drying, *e* and *f* — LFP/C particles obtained using different carbon sources, *g*—*i* — LFP/C particles at different magnification: general view (*g*), individual particle (*h*), and the porous structure of the particle (*i*).

Table 2. Characteristics of spherical LFP particles obtained by different methods

Method	Starting components	ρ/g cm^{-3}	Discharge cpacity /mA h g^{-1} (current density)	Reference
Precipitation	$Fe(NO_3)_3$, H_3PO_4, Li_2CO_3	1.60	150 (0.1C)	112
Precipitation	$Fe(NO_3)_3$, H_3PO_4, Li_2CO_3	1.60	152 (0.4C); 110 (4C)	113
Ball milling/spray drying/ carbothermal reduction	$FePO_4$, Li_2CO_3	1.68	164 (0.2C)	116
Sol-gel/spray drying /annealing	$FeC_6H_5O_7 \cdot 5H_2O$, $NH_4H_2PO_4$, Li_2CO_3	1.53	162.5 (0.1C)	120
Precipitation	H_3PO_4, $Fe(NO_3) \cdot 9H_2O$, Li_2CO_3	**1.80**	167 (0.1C)	121
Solid-phase synthesis /spray drying	$FePO_4$, Li_2CO_3	1.21	162.19 (0.2C); 156.38 (1C)	122
Hydrothermal synthesis	H_3PO_4, $Fe(NO_3) \cdot 9H_2O$, LiOH	1.40	162 (0.1C); 116 (10C)	123
Hydrothermal synthesis	$Fe(NO_3) \cdot 6\ H_2O$, $NH_4H_2PO_4$, $LiOAc \cdot 2H_2O$	1.40	153 (0.1C); 115 (10C)	124
Solvothermal synthesis	LiH_2PO_4, $FeSO_4 \cdot 7H_2O$	1.40	132.5 (0.1C)	125
Solvothermal synthesis	$FeSO_4 \cdot 7H_2O$, H_3PO_4, $LiNO_3$	1.50	158 (0.1C); 109 (5C)	126
Microwave heating/ hydrothermal synthesis/ carbothermal reduction	LiH_2PO_4, $C_6H_5FeO_7$	1.30	160 (0.1C)	127
Precipitation	LiH_2PO_4, $Fe(OAc)_2$	**1.82**	165 (0.1C); 48 (10C)	128

density and, therefore, specific volumetric energy. An analysis of the photomicrographs in Fig. 8 suggests that secondary micrometer-sized LFP particles can also be synthesized by different methods (or their combination). Porosity of spherical particles is of paramount importance because pores allow the electrolyte to diffuse into the interior of the particle, thus increasing the proportion of the active material involved in the electrochemical processes. Besides, it is important to retain high density of particles in order to maintain high bulk density.

Among all methods for the synthesis of LFP mentioned above, precipitation of precursor followed by spray drying is the most promising approach from the standpoint of synthesis of spherical particles. The method requires is simple to implement, efficiently utilizes inexpensive and readily available raw materials, and makes it possible to obtain particles with the highest bulk density that are used in producing LIBs characterized by the highest volumetric energy density. When iron sources contain the metal in the highest oxidation state (*i.e.*, Fe^{+3}), the precipitation process is usually carried out in air under continuous stirring at atmospheric pressure. The size of precipitate particles is inversely proportional to the concentrations of the starting reagents and therefore can be efficiently controlled in order to form the optimum structure.

The bulk densities and specific parameters of spherical LFP particles synthesized by different methods are compared in Table 2.

It should be noted that the published LFP bulk density values can be abnormally high.[121,128] Probably, in this case one deals with the tap density of LFP, which is much higher than the bulk density of the synthesized materials.

Precipitation methods for the synthesis of high-performance cathode materials: specific features of practical application

From the standpoint of the cost of reagents, the metal consumption of equipment, and the number of intermediate technological steps, the precipitation of iron phosphate followed by sintering with the lithium source is one of the cheapest methods for the synthesis of LFP having high electrochemical performance.

Table 3 lists the systematized literature data on the types of the raw materials, sintering (calcination) temperatures, and specific discharge capacities of the resulting LFP.

Common to all processes under study are the ranges of the medium pH values, the solution temperatures at which precipitation occurs, and the concentrations of the interacting components (Fig. 9).

Table 3. Synthesis conditions of $LiFePO_4$ by the precipitation method

Iron source	Phosphorus source	Lithium source	Carbon source	T/°C	Discharge capacity/mA h g^{-1} (current density)	Reference
$Fe(NO_3)_3$	$(NH_4)_2HPO_4$	Li_2CO_3	Glucose	600	162.5 (0.1C)	64
$FeSO_4$	$NH_4H_2PO_4$	Li_2CO_3	Glucose	650	162.7(0.1C)	86
$FeSO_4$	H_3PO_4	Li_2CO_3	Glucose	700	144.8 (0.1C)	130
$FeSO_4$	LiH_2PO_4	LiH_2PO_4	Glucose	700	159 (0.1C)	131
$FeSO_4$	H_3PO_4	Li_2CO_3	Oxalic acid	500	166 (0.1C)	132
$(NH_4)_2Fe(SO_4)_2$	$NH_4H_2PO_4$	LiOH	Graphene	700	160 (0.2C)	133
$Fe(NO_3)_3$	Na_2HPO_4	LiI	—	550	153 (C/7)	134
$FeSO_4$	$(NH_4)_2H_2PO_4$	Li_2CO_3	Glucose	650	157.79 (0.1C)	135
$FeSO_4$	$NH_4H_2PO_4$	Li_2NO_3	Activated carbon	550	163 (0.1C)	136
$FeSO_4$	$NH_4H_2PO_4$	Li_3PO_4	Citric acid	600	163.3 (0.2C)	137
$FeSO_4$	H_3PO_4	Li_2CO_3	Glucose	700	158.4 (0.2C)	138
$FeSO_4$	NaH_2PO_4	Li_2CO_3	Glucose	750	163.7 (0.1C)	139
$FeSO_4$	H_3PO_4	LiOH	Glucose	650	155 (0.1C)	140
$FeSO_4$	$(NH_4)_2HPO_4$	$LiNO_3$	Stearic acid	700	160 (0.1C)	141
$FeCl_3$	H_3PO_4	LiOH	Glucose	650	141.4 (0.5C)	142
$Fe(NO_3)_3$	H_3PO_4	Li_2CO_3	Glucose	700	163.9 (0.1C)	143
$Fe(NO_3)_3$	H_3PO_4	Li_2CO_3	Glucose	700	146 (0.1C)	144

Using the corresponding data within the ranges specified, one can choose the optimum synthesis conditions for all combinations of raw materials and available equipment.

Most studies on the sintering of iron phosphate with lithium sources report the actual temperatures at which products with the best electrochemical performance are formed. Emphasize that these values can differ from one another depending on the design of the oven; however, the optimum sintering temperature most probably falls in the range specified (see Fig. 9). The synthesis of lithium iron phosphate

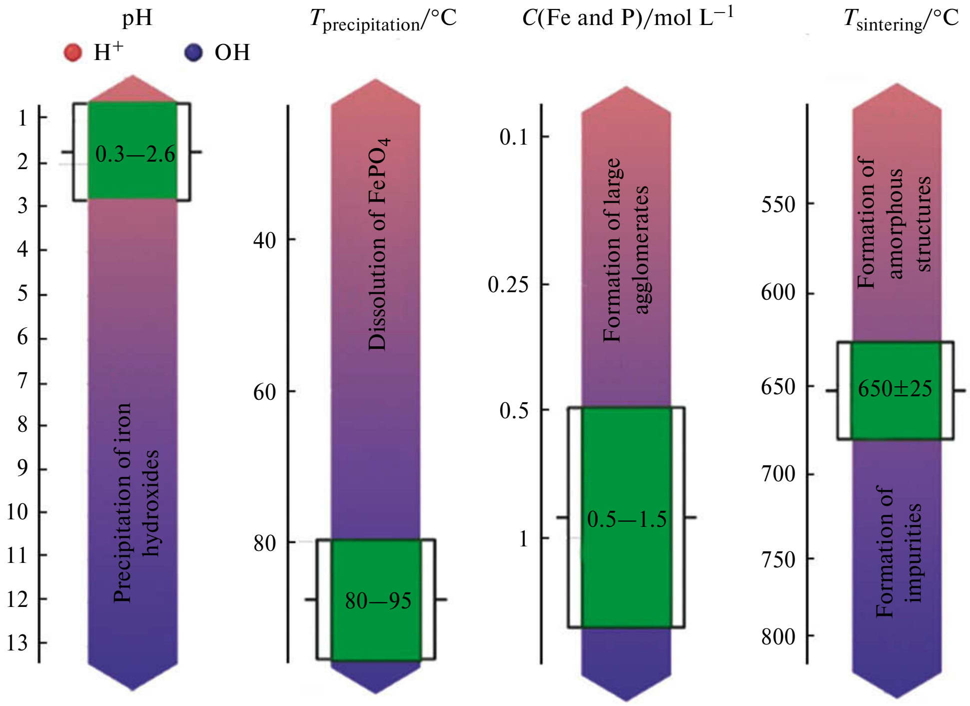

Fig. 9. Optimum parameters of the synthesis of lithium iron phosphate (LFP) by the precipitation method.

using the intermediate precipitation step is aimed at obtaining a single-phase, defect-free material consisting of micrometer-sized spherical particles with uniform carbon coating.

Conclusion

In this work we considered specific features of various methods for the synthesis of lithium iron phosphate having high electrochemical performance. It was established that the most promising methods include precipitation of iron phosphate followed by spray drying and hydrothermal synthesis. Both of them are rather simple to implement.

Usually, most studies are devoted to the effect of a certain parameter on the electrochemical properties of cathode materials (other things being equal), while other parameters are not optimal, although remain unchanged and thus do not influence the final result. Our analysis of the relevant literature made it possible to generalize and systematize the data on optimization of the precipitation conditions of $FePO_4$ and methods for the synthesis of materials with the best electrochemical performance as well as to reveal some trends in the effects of the properties of the starting reagents and methods for the synthesis of LEP on the final operating parameters of these materials.

Summing up, the development of an efficient method for the synthesis of cathode materials using the precipitation technique involves substantiated choice of the synthesis conditions and a search for balance between different operating properties of the resulting materials. Although the key parameters of the synthesis can be varied within narrow ranges, one can successfully obtain materials with desired properties.

Funding

This work was financially supported by the Russian Science Foundation (Project No. 22-73-00246; https://rscf.ru/project/22-73-00246/).

Animal Testing and Ethics

No human or animal subjects were used in this research.

Conflict of Interest

The authors declare no competing interests.

References

1. D. Choi, N. Shamim, A. Crawford, Q. Huang, Ch. K. Vartanian, V. V. Viswanathan, M. D. Paiss, Md J. E. Alam, D. Reed, V. Sprenkle, *J. Power Sources*, 2021, **511**, 230419; DOI: 10.1016/j.jpowsour.2021.230419.
2. H. Lund, *Energy*, 2007, **32**, 6, 912-919; DOI: 10.1016/j.energy.2006.10.017.
3. Erdiwansyah, Mahidin, H. Husin, Nasaruddin, M. Zaki, M. Erdiwansyah. *Prot. Control. Mod. Power Syst.*, 2021, **6**, 3; DOI: 10.1186/s41601-021-00181-3.
4. J. Hu, L. Li, E. Hu, S. Chae, H. Jia, T. Liu, B. Wu, Y. Bi, K. Amine, C. Wang, J. Zhang, J. Tao, J. Xiao, *Nano Energy*, 2021, **79**, 105420; DOI: 10.1016/j.nanoen.2020.105420.
5. Y. Li, Y.-F. Du, G.-H. Sun, *Eco Mat.* 2021, **3**, 312091; DOI: 10.1002/eom2.12091.
6. C. M. Costa, J. C. Barbosa, R. Gonçalves, H. Castro, F. J. Del Campo, S. Lanceros-Méndez, *Energy Storage Mater.*, 2021, **37**, 433; DOI: 10.1016/j.ensm.2021.02.032.
7. X. Zhang, Z. Li, L. Luo, Y. Fan, Z. Du, *Energy*, 2022, **238**, 121652; DOI: 10.1016/j.energy.2021.121652.
8. W. Li, Y.-G. Cho, W. Yao, Y. Li, A. Cronk, R. Shimizu, M. A. Schroeder, Ya. Fu, F. Zou, V. Battaglia, A. Manthiram, M. Zhang, Y. Sh. Meng, *J. Power Sources*, 2020, **473**, 228579; DOI: 10.1016/j.jpowsour.2020.228579.
9. M. Freire, N. Kosova, C. Jordy, D. Chateigner, O. I. Lebedev, A. Maignan, V. Pralong, *Nature Mater.*, 2016, **15**, 173—177; DOI: 10.1038/nmat4479.
10. S. Bourlot, P. Blanchard, S. Robert, *J. Power Sources*, 2011, **196,** 6841; DOI: 10.1016/j.jpowsour.2010.09.103.
11. L. Unterreiner, V. Jülch, S. Reith, *Energy Proc.*, 2016, **99**, 229; DOI: 10.1016/j.egypro.2016.10.113.
12. D. Miranda, C. M. Costa, S. Lanceros-Mendez, *J. Electroanal. Chem.*, 2015, **739**, 97; DOI: 10.1016/j.jelechem.2014.12.010.
13. Zh. J. Zhang, PremanandRamadass, W. Fang, *18 — Safety of Lithium-Ion Batteries Lithium-Ion Batteries*, Elsevier, 2014, 409; DOI: 10.1016/B978-0-444-59513-3.00018-2.
14. Z. Li, D. Zhang, F. Yang, *J. Mater. Sci.*, 2009, **44**, 2435; DOI: 10.1007/s10853-009-3316-z.
15. Y. Xu, Y. Dong, X. Han, X. Wang, Y. Wang, L. Jiao, H. Yuan, *ACS Sust. Chem. Eng.*, 2015, **3**, 2435; DOI: 10.1021/acssuschemeng.5b00455.
16. M. Wang, Q. Tan, L. Liu, J. Li, *J. Hazard. Mater.*, 2019, **380**, 120846; DOI: 10.1016/j.jhazmat.2019.120846.

17. S. Sharma, A. Manthiram, *Energy Environ. Sci.*, 2020, **13**, 4087; DOI: 10.1039/d0ee02511a.
18. Y. Miao, P. Hynan, A. von Jouanne, A. Yokochi, *Energies*, 2019, **12**, 1074; DOI: 10.3390/en12061074.
19. W.-J. Zhang, *J. Power Sources*, 2011, **196**, 2962; DOI: 10.1016/j.jpowsour.2010.11.113.
20. A. Eftekhari, *J. Power Sources*, 2017, **343**, 395; DOI: 10.1016/j.jpowsour.2017.01.080.
21. H. Zhang, Zh. Zou, Sh. Zhang, J. Liu, Sh. Zhong, *Int. J. Electrochem. Sci.*, 2020, **15**, 12041; DOI: 10.20964/2020.12.71.
22. W. F. Howard, R. M. Spotnitz, *J. Power Sources*, 2007, **165**, 887; DOI: 10.1016/j.jpowsour.2006.12.046.
23. Y. Zhang, Q.-y. Huo, P.-p. Du, L.-zh. Wang, A.-q. Zhang, Y.-h. Song, Y. Lv, G.-y. Li, *Synth. Metals*, 2012, **162**, 13—14, 1315 DOI: 10.1016/j.synthmet.2012.04.025.
24. P. M. Pratheeksha, E. H. Mohan, B. V. Sarada, M. Ramakrishna, K. Hembram, P. V. Venkata Srinivas, P. J. Daniel, T. N. Rao, S. Anandan, *Phys. Chem. Chem. Phys.,* 2017, **19.1**, 175; DOI: 10.1039/C6CP06923A.
25. K. Naoi, K. Kisu, E. Iwama, S. Nakashima, Y. Sakai, Y. Orikasa, P. Leone, N. Dupré, T. Brousse, P. Rozier, W. Naoi, P. Simon, *Energy Environ. Sci.*, 2016, **9**, 2143; DOI :10.1039/c6ee00829a.
26. S. H. Ha, Y. J. Lee, *Chem.—Eur. J.*, 2014, **21**, 2132; DOI: 10.1002/chem.201404952.
27. C. Huang, T. Kuo, S. Yougbaré, L. Lin, *J. Colloid Interface Sci.*, 2022, **607**, 1457; DOI: 10.1016/j.jcis.2021.09.118.
28. Z. Li, J. Yang, T. Guang, B. Fan, K. Zhu, X. Wang, *Small Methods*, 2021, **5**, 2100193; DOI: 10.1002/smtd.202100193.
29. J. Xue, Z. Zhang, H. Guo, R. Liu, Y. Wang, L. Wen, G. Liang, *Ionics*, 2022, **28**, 4229—4237; DOI: 10.1007/s11581-022-04632-1.
30. D. Xu, X. Chu, Y. He, Z. Ding, B. Li, W. Han, H. Du, F. Kang, *Electrochim. Acta*, 2015, **152**, 398; DOI: 10.1016/j.electacta.2014.11.025.
31. C. Qiu, L. Liu, F. Du, X. Yang, C. Wang, G. Chen, Y. Wie, *Chem. Res. Chin. Univ.*, 2015, **31**, 270; DOI: 10.1007/s40242-015-4367-0.
32. Y. Azizi, S. M. Sadrameli, *Energy Conv. Manag.*, 2016, **128**, 294; DOI: 10.1016/j.enconman.2016.09.081.
33. F. Yu, J. Zhang, Y. Yang, G. Song, *J. Power Sources*, 2010, **195**, 19, 6873; DOI: 10.1016/j.jpowsour.2010.01.042.
34. D. Jugović, D. Usković, *J. Power Sources*, **190**, 2, 538; DOI: 10.1016/j.jpowsour.2009.01.074.
35. Y. Zhang, Q. Huo, P. Du, L. Wang, A. Zhang, Y. Song, Y. Lv, G. Li, *Synth. Metals*, 2012, **162**, 1315; DOI: 10.1016/j.synthmet.2012.04.025.
36. T. V. S. L. Satyavani, A. Srinivas Kumar, P. S. V. Subba Rao, *Eng. Sci. Technol. Int. J.*, 2016, **19**, 178; DOI: 10.1016/j.jestch.2015.06.002.
37. D.-H. Seo, K.-Y. Park, H. Kim, S.-K. Jung, M.-S. Park, K. Kang, *Adv. Energy Mater.*, 2018, **8**, 1701408; DOI: 10.1002/aenm.201701408.
38. D. Vernardou, *Coatings*, 2022, **12**, 1543; DOI: 10.3390/coatings12101543.
39. V. Sreeja, P. A. Joy, *Mater. Res. Bull.*, 2007, **42**, 1570; DOI: 10.1016/j.materresbull.2006.11.014.
40. N. Bai, H. Chen, W. Zhou, K. Xiang, Y. Zhang, C. Li, H. Lu, *Electrochim. Acta*, 2015, **167**, 172; DOI: 10.1016/j.electacta.2015.03.163.
41. A. Kulka, K. Walczak, W. Zając, J. Molenda, *J. Solid State Chem.*, 2017, **253**, 367; DOI: 10.1016/j.jssc.2017.06.022.
42. X. Pan, Y. Sun, S. Zhuang, G. Sun, S. Jiang, Y. Ren, Y. Wen, X. Li, F. Tu, *Vacuum*, 2023, **212**, 112258; DOI: 10.1016/j.vacuum.2023.112258.
43. G. Liu, S. Zhang, X. Wei, S. Wang, Y. Yu, *Int. J. Electrochem. Sci.*, 2016, **11**, 6799; DOI: 10.20964/2016.08.28.
44. J. Cui, Y. Du, H. Xiao, Q. Yi, D. Du, *Hydrometallurgy*, 2014, **146**, 169; DOI: 10.1016/j.hydromet.2014.03.012.
45. O. Gileva, P. Aryal, S. Karki, H. Kim, Y. Kim, V. Milyutin, H. Park, K. Shin, *J. Radioanal. Nucl. Chem.*, 2017, **314**, 1695; DOI: 10.1007/s10967-017-5568-4.
46. S. Sun, S. Wang, Y. Ye, B. Pan, *Water Res.*, 2019, **153**, 21; DOI: 10.1016/j.watres.2019.01.007.
47. V.N. Bulut, C. Duran, A. Gundogdu, M. Soylak, N. Yildirim, L. Elci, *Talanta*, 2008, **76**, 469; DOI: 10.1016/j.talanta.2008.03.040.
48. L. Kouisni, M. Azzi, M. Zertoubi, F. Dalard, S. Maximovitch, *Surface Coat. Technol.*, 2004, **185**, 58; DOI: 10.1016/j.surfcoat.2003.10.061.
49. L. Ying, L. Xia Wang, D. Lu, J. Sun, J. C. Sun, *Key Eng. Mater.*, 2012, **519**, 132; DOI: 10.4028/www.scientific.net/kem.519.132.
50. I. Mahmud, DS. Kim, S. C. Ur, *J. Korean Phys. Soc.*, 2016, **68**, 1211; DOI: 10.3938/jkps.68.1211.
51. L. Wu, X. Li, Z. Wang, L. Li, J. Zheng, H. Guo, Q. Hu, J. Fang, *J. Power Sources*, 2009, **189**, 681; DOI: 10.1016/j.jpowsour.2008.08.097.
52. F. Gao, Z. Tang, J. Xue, *J. Univer. Sci. Technol. Beijing, Mineral, Metall., Mater.*, 2008, **15**, 802; DOI: 10.1016/S1005-8850(08)60291-1.
53. R. Qi, Z. Xu, Y. Zhou, D. Zhang, Z. Sun, W. Chen, M. Xiong, *Energy*, 2021, **214**, 118926; DOI: 10.1016/j.energy.2020.118926.
54. J. Li, J. Wu, Y. Li, H. Zhao, T. Zhao, S. Ma, H. Liu, *J. Taiwan Institute Chem. Eng.*, 2019, **99**, 74; DOI: 10.1016/j.jtice.2019.03.002.
55. B. Q. Zhu, X. H. Li, Z. X. Wang, H. J. Guo, *Mater. Chem. Phys.*, 2006, **98**, 373; DOI: 10.1016/j.matchemphys.2005.09.046.
56. J. Li, Z.-F. Ma, *Chemistry*, 2019, **5**, 3; DOI: 10.1016/j.chempr.2018.12.012.

57. Z. Cao, B. Ma, C. Wang, B. Shi, Y. Chen, *Hydrometallurgy*, 2022, **212**, 105896; DOI: 10.1016/j.hydromet.2022.105896.
58. K. Kandori, T. Kuwae, T. Ishikawa, *J. Colloid Interface Sci.*, 2006, **300**, 225; DOI: 10.1016/j.jcis.2006.03.072.
59. Y. Lu, T. Zhang, Y. Liu, G. Luo, *Chem. Eng. J.*, 2012, **210**, 18; DOI: 10.1016/j.cej.2012.08.077.
60. J. Thistleton, T.-A. Berry, P. Pearce, S.A. Parsons, *Process Safety Environ. Protect.*, 2002, **80**, 265; DOI: 10.1205/095758202762277623.
61. W. Lou, Y. Zhang, Y. Zhang, S. Zheng, P. Sun, X. Wang, S. Qiao, J. Li, Y. Zhang, D. Liu, M. Wenzel, J. J. Weigand, *J. Alloys Compd.*, 2021, **856**, 158148; DOI: 10.1016/j.jallcom.2020.158148.
62. C. Huang, D. Ai, L. Wang, X. He, *Int. J. Electrochem. Sci.*, 2016, **11**, 754—762. DOI: 10.1016/S1452-3981(23)15881-0.
63. L. Wang, X. He, W. Sun, J. Wang, Y. Li, S. Fan, *Nano Lett.*, 2012, **12**, 5632; DOI: 10.1021/nl3027839.
64. Y. Zhu, S. Tang, H. Shi, H. Hu, *Ceram. Inter.*, 2014, **40**, 2685; DOI: 10.1016/j.ceramint.2013.10.055.
65. X. Zhang, K. Zhou, D. Zeng, J. Li, Y. Wu, W. Chen, C. Peng, *Bull. Environ. Contam. Toxicol.*, 2022, **109**, 86; DOI: 10.1007/s00128-022-03472-z.
66. X. Zhang, K. Zhou, Q. Lei, Y. Huang, C. Peng, W. Chen, *J. Miner., Metal. Mater. Soc.*, 2019, **71**, 4608; DOI: 10.1007/s11837-019-03801-4.
67. M. Balintova, A. Petrilakova, *Chem. Eng. Trans.*, 2011, **25**, 1—6; DOI: 10.3303/CET1125058.
68. C. Hsieh, I. L. Chen, W. Chen, J. Wang, *Electrochim. Acta*, 2012, **83**, 202; DOI: 10.1016/j.electacta.2012.07.108.
69. X.-X. Zhang, S.-S. Tang, M.-L. Chen, J.-H. Wang, *J. Anal. At. Spectrom.*, 2012, **27**, 466; DOI: 10.1039/C2JA10292G.
70. Y. Song, H. H. Hahn, E. Hoffmann, *Chemosphere*, 2002, **48**, 1029; DOI: 10.1016/S0045-6535(02)00183-2.
71. T. Maqbool, P. Srikiratiwong, H. S. Fogler, *Energy & Fuels*, 2011, **25**, 694; DOI: 10.1021/ef101112r.
72. J. Wang, J. Li, Q. Wang, J. Wang, Z. Wang, C. T. Liu, *Scripta Mater.*, 2019, **168**, 19; DOI: 10.1016/j.scriptamat.2019.04.013.
73. M. Covarrubias-Cervantes, S. Bongard, D. Champion, A. Voilley, *LWT — Food Sci. Technol.*, 2005, **38**, 371; DOI: 10.1016/j.lwt.2004.06.015.
74. Y. Xiao, Z. Zhen, H. P. Wie, *Adv. Mater. Res.*, 2014, **875—877**, 95; DOI: 10.4028/www.scientific.net/amr.875-877.95.
75. L. Yang, Y. Feng, C. Wang, D. Fang, G. Yi, Z. Gao, P. Shao, C. Liu, X. Luo, S. Luo, *Chem. Eng. J.*, 2022, **431**, 1385; DOI: 10.1016/j.cej.2021.133232.
76. T. Roncal-Herrero, J. D. Rodríguez-Blanco, L. G. Benning, E. H. Oelkers, *Cryst. Growth Design*, 2009, **9**, 5197; DOI: 10.1021/cg900654m.
77. A. Dickson, J. Riley, *Marine Chem.*, 1979, **7**, 101—109; DOI: 10.1016/0304-4203(79)90002-1.
78. C. Wang, Y. Xunlong, T. Huiyun, J. Shuofeng, M. Ziting, Z. Junjie, W. Xuewen, C. Dapeng, D. Yifan, *Coatings*, 2021, **11**, 1137; DOI: 10.3390/coatings11091137.
79. S. Deng, H. Wang, H. Liu, J. Liu, H. Yan, *Nano-Micro Lett.*, 2014, **6**, 209; DOI: 10.1007/BF03353785.
80. S. B. Lee, S. H. Cho, S. J. Cho, G. J. Park, S. H. Park, Y. S. Lee, *Electrochem. Commun.*, 2008, **10**, 1219; DOI: 10.1016/j.elecom.2008.06.007.
81. H. Li, L. Peng, D. B. Wu, J. Wu, Y.-J. Zhu, X. L. Hu, *Adv. Energy Mater.*, 2019, **9**, 1802930; DOI: 10.1002/aenm.201802930.
82. H. Liu, P. Zhang, G. C. Li, Q. Wu, Y. P. Wu, *J. Solid State Electrochem*, 2008, **12**, 1011; DOI: 10.1007/s10008-007-0478-y.
83. Q. Fan, L. Lei, X. Xu, G. Yin, Y. Sun, *J. Power Sources*, 2014, **257**, 65; DOI: 10.1016/j.jpowsour.2014.01.044.
84. W. Peng, L. Jiao, H. Gao, Z. Qi, Q.Wang, H. Du, Y. Si, Y. Wang, H. Yuan, *J. Power Sources*, 2011, **196**, Issue 5, 2841; DOI: 10.1016/j.jpowsour.2010.10.065.
85. T. T. Zhan, W. F. Jiang, C. Li, X. D. Luo, G. Lin, Y. W. Li, S. H. Xiao, *Electrochim. Acta*, 2017, **246**, 322; DOI: 10.1016/j.electacta.2017.05.151.
86. G. Hu, X. Xie, Z. Peng, K. Du, Z. Gan, L. Xu, Y. Wang, Y. Cao, *Solid State Ionics*, 2019, **340**, 115014; DOI: 10.1016/j.ssi.2019.115014.
87. F. Yang, H. Zhang, Y. Shao, H. Song, S. Liao, J. Ren, *Ceram. Inter.*, 2017, **43**, 16652; DOI: 10.1016/j.ceramint.2017.09.055.
88. A.T. Phan, A.E. Gheribi, P. Chartrand, *Can. J. Chem. Eng.*, 2018, **97**, 2224; DOI: 10.1002/cjce.23416.
89. B. Chen, M. Liu, S. Cao, G. Chen, X. Guo, X. Wang, *Mater. Chem. Phys.*, 2022, **279**, 125750; DOI: 10.1016/j.matchemphys.2022.125750.
90. C. W. Kim, J. S. Park, K. S. Lee, *J. Power Sources*, 2006, **163**, 144; DOI: 10.1016/j.jpowsour.2006.02.071.
91. L. Wang, Y. Huang, R. Jiang, D. Jia, *Electrochim. Acta*, 2007, **52**, 6778; DOI: 10.1016/j.electacta.2007.04.104.
92. S. Vedala, M. Sushama, *Mat. Tod.: Proc.*, 2018, **5**, 1649, DOI: 10.1016/j.matpr.2017.11.259.
93. Z. Liu, J. Li, Y. Xing, L. Wang, S. Fang, B. Xu, X. Qu, *Ionics,* 2014, **20**, 1511; DOI: 10.1007/s11581-014-1110-7.
94. Z. Q. Hu, D. X. Yang, K. J. Yin, J. X. Liu, F. Li, W. Y. Gao, Y. Qin, H. Liu, *Adv. Mater. Res.*, 2013, **669**, 311; DOI: 10.4028/www.scientific.net/amr.669.311.
95. O. Toprakci, H. A. K. Toprakci, L. Ji, X. Zhang, *KONA Powder and Particle J.*, 2010, **28**, 50—73; DOI: 10.14356/kona.2010008.
96. Y. E. Milián, N. Reinaga, M. Grágeda, S. Ushak, *J. Sol-Gel Sci. Technol.*, 2020, **94**, 22; DOI: 10.1007/s10971-019-05090-4.
97. J. J. Ma, J. Zhou, X. M. Zu, X. Y. Wang, *Adv. Mater. Res.*, 2015, **1120—1121**, 128; DOI: 10.4028/www.scientific.net/amr.1120-1121.128.

98. Z. Chen, H. Zhu, S. Ji, R. Fakir, V. Linkov, *Solid State Ionics*, 2008, **179**, 1810; DOI: 10.1016/j.ssi.2008.04.018.
99. M. M. Doeff, J. D. Wilcox, R. Kostecki, G. Lau, *J. Power Sources*, 2006, **163**, 180; DOI: 10.1016/j.jpowsour.2005.11.075.
100. F. Gao, Z. Tang, J. Xue, *Electrochim. Acta*, 2007, **53**, 1939; DOI: 10.1016/j.electacta.2007.08.048.
101. C.-Z. Lu, G. Ting-Kuo Fey, H.-M. Kao, *J. Power Sources*, 2009, **189**, 155; DOI: 10.1016/j.jpowsour.2008.10.015.
102. Y.-D. Cho, G. Ting-Kuo Fey, H.-M. Kao, *J. Power Sources*, 2009, **189**, 256; DOI: 10.1016/j.jpowsour.2008.09.053.
103. H. C. Shin, W. Cho, H. Jang, *Electrochim. Acta*, 2006, **52**, 1472; DOI: 10.1016/j.electacta.2006.01.078.
104. T. Wu, X. Ma, X. Liu, G. Zeng, W. Xiao, *Mater. Technol.*, 2015, **30**, A70; DOI: 10.1179/17535557A15Y.000000011.
105. Y. Z. Dong, Y. M. Zhao, Y. H. Chen, Z. F. He, Q. Kuang, *Mater. Chem. Phys.*, 2099, **115**, 245; DOI: 10.1016/j.matchemphys.2008.11.063.
106. L. Wang, G. C. Liang, X. Q. Ou, X. K. Zhi, J. P. Zhang, J. Y. Cui, *J. Power Sources*, 2009, **189**, 423; DOI: 10.1016/j.jpowsour.2008.07.032.
107. G.Xie, H.-J.Zhu, X.-M. Liu, H. Yang, *J. Alloys Compd.*, 2013, **574**, 155; DOI: 10.1016/j.jallcom.2013.03.281.
108. Y. Zhang, H. Shi, Q. Meng, Y. Yao, P. Dong, D. Wang, J. Duan, B. Xu, *Ionics*, 2020, **26**, 4949; DOI: 10.1007/s11581-020-03664-9.
109. C. Miao, P. Bai, Q. Jiang, S. Sun, X. Wang, *J. Power Sources*, 2014, **246**, 232; DOI: 10.1016/j.jpowsour.2013.07.077.
110. H. B. Gu, D. K. Jun, G. C. Park, B. Jin, E. M. Jin, *J Nanosci. Nanotechnol.*, 2007, **7**, 3980; DOI: 10.1166/jnn.2007.079.
111. X. Gao, G. Hu, Z. Peng, K. Du, *Electrochim. Acta*, 2009, **54**, 4777; DOI: 10.1016/j.electacta.2008.12.024.
112. S. W. Oh, S.-T. Myung, S.-M. Oh, C. S. Yoon, K. Amine, Y.-K. Sun, *Electrochim. Acta*, 2010, **55**, 1193; DOI: 10.1016/j.electacta.2009.10.007.
113. H.-M. Xie, R.-S. Wang, J.-R. Ying, L.-Y. Zhang, A. F. Jalbout, H.-Y. Yu, G.-L. Yang, X.-M. Pan, Z.-M. Su, *Adv. Mater.*, 2006, **18**, 2609; DOI: 10.1002/adma.200600578.
114. J. Ying, C. Jiang, C. Wan, *J. Power Sources*, 2004, **129**, 264; DOI: 10.1016/j.jpowsour.2003.10.007.
115. J. Lim, V. Mathew, K. Kim, J. Moon, J. Kim, *J. Electrochem. Soc.*, 2011, **158**, A736. DOI: 10.1149/1.3581029.
116. X. Wang, L. Wen, Y. Zheng, H. Liu, G. Liang, *Ionics*, 2019, **25**, 4589; DOI: 10.1007/s11581-019-03025-1.
117. C. Yan, K. Wu, P. Jing, H. Luo, Y. Zhang, *Mater. Chem. Phys.*, 2022, **280**, 125711; DOI: 10.1016/j.matchemphys.2022.125711.
118. Y. Ma, T. Li, F. Jiang, Y. Jiang, F. Gao, L. Liu, Y. Wu, Y. Meng, X. Ma, Z. Zi, *Int. J. Electrochem. Sci.*, 2022, **17**, 220453; DOI: 10.20964/2022.04.32.
119. J. Sun, Z. Li, X. Ren, L. Wang, G. Liang, *J. Alloys Compd.*, 2019, **773**, 788; DOI: 10.1016/j.jallcom.2018.09.215.
120. L. Wu, S.-K. Zhong, J.-Q. Liu, F. Lv, K. Wan, *Mater. Lett.*, 2012, **89**, 32; DOI: 10.1016/j.matlet.2012.08.076.
121. Z.-R. Chang, H.-J. Lv, H.-W. Tang, H.-J. Li, X.-Z. Yuan, H. Wang, *Electrochim. Acta*, 2009, **54**, 4595; DOI: 10.1016/j.electacta.2009.03.063.
122. L. Chen, Z. Chen, S. Liu, H. Zhang, Q. Huang, *Int. J. Electrochem. Sci.*, 2018, **13**, 5413; DOI: 10.20964/2018.06.21.
123. X. Lou, Y. Zhang, *J. Mater. Chem.*, 2011, **21**, 4156; DOI: 10.1039/C0JM03331F.
124. J. Qian, M. Zhou, Y. Cao, X. Ai, H. Yang, *J. Phys. Chem. C*, 2010, **114**, 3477; DOI: 10.1021/jp912102k.
125. Y. Jin, X. Tang, H. Wang, *RSC Adv.*, 2016, **6**, 75602; DOI: 10.1039/C6RA13907H.
126. J. Guo, L. Chen, X. Zhang, H. Chen, L. Tang, *Mater. Lett.*, 2013, **106**, 290; DOI: 10.1016/j.matlet.2013.05.044.
127. R. Chen, Y. Wu, X. Y. Kong, *J. Power Sources*, 2014, **258**, 246; DOI: 10.1016/j.jpowsour.2014.02.068.
128. N. Bai, H. Chen, W. Zhou, K. Xiang, Y. Zhang, C. Li, H. Lu, *Electrochim. Acta*, 2015, **167**, 172; DOI: 10.1016/j.electacta.2015.03.163.
129. K. S. Park, K. T. Kang, S. B. Lee, G. Y. Kim, Y. J. Park, H. G. Kim, *Mater. Res. Bull.*, 2004, **39**, 1803; DOI: 10.1016/j.materresbull.2004.07.003.
130. Y.-J. Wu, Y.-J. Gu, Y.-B. Chen, H.-Q. Liu, C.-Q. Liu, *Inter. J. Hydrogen Energy*, 2018, **43**, 2050; DOI: 10.1016/j.ijhydene.2017.12.061.
131. Y. Liu, C. Cao, *Electrochim. Acta*, 2010, **55**, 4694; DOI: 10.1016/j.electacta.2010.03.033.
132. J. Zheng, X. Li, Z. Wang, H. Guo, S. Zhou, *J. Power Sources*, 2008, **184**, 574; DOI: 10.1016/j.jpowsour.2008.01.016.
133. Y. Ding, Y. Jiang, F. Xu, J. Yin, H. Ren, Q. Zhuo, Z. Long, P. Zhang, *Electrochem. Commun.*, 2010, **12**, 10; DOI: 10.1016/j.elecom.2009.10.023.
134. R. Trócoli, J. Morales, J. Santos Peña, *Solid State Ionics*, 2014, **255**, 30; DOI: 10.1016/j.ssi.2013.11.038.
135. T. Zhang, D. Gong, S. Lin, J. Yu, *Chem. Eng. J.*, 2022, **449**, 137830; DOI: 10.1016/j.cej.2022.137830.
136. A. H. Omidi, A. Babaei, A. Ataie, *Mater. Res. Bull.*, 2020, **125**, 110807; DOI: 10.1016/j.materresbull.2020.110807.
137. Y. Wang, J. Zhang, S. Tian, J. Xue, L. Wen, G. Liang, *Ionics*, 2021, **27**, 993; DOI: 10.1007/s11581-020-03881-2.
138. X. Wang, L. Wen, Y. Zheng, X. Ren, Y. Li, G. Liang, *Ionics*, 2020, **26**, 4433; DOI: 10.1007/s11581-020-03594-6.

139. X. Yan, Y. Yang, C. Li, J. Liu, J. Wang, F. Xi, T. Wang, W. He, *Ionics*, 2022, **28**, 1559; DOI: 10.1007/s11581-021-04430-1.
140. S. Wang, H. Yang, L. Feng, S. Sun, J. Guo, Y. Yang, H. Wei, *J. Power Sources*, 2013, **233**, 43; DOI: 10.1016/j.jpowsour.2013.01.124.
141. D. Jugović, M. Mitrić, M. Kuzmanović, N. Cvjetićanin, S. Škapin, B. Cekić, V. Ivanovski, D. Uskoković, *J. Power Sources*, 2011, **196**, 4613; DOI: 10.1016/j.jpowsour.2011.01.072.
142. W. K. Zhang, H. J. Zeng, Y. Xia, L. C. Qian, B. Zhao, H. Huang, Y. P. Gan, X. Y. Tao, *Adv. Mater. Res.*, 2011, **399—401**, 1510; DOI: 10.4028/www.scientific.net/amr.399-401.1510.
143. X. Qin, G. Yang, F. Ma, F. Cai, *Russ. J. Phys. Chem.*, 2016, **90**, 233—239; DOI: 10.1134/S0036024415120304.
144. Y. J. Gu, P. Liu, Y. B. Chen, H. Q. Liu, Y. M. Wang, F. X. Hao, Q. G. Zhang, S. Q. Li. *Adv. Mater. Res.*, 2013, **643**, 100; DOI: 10.4028/www.scientific.net/AMR.643.100.

Received May 2, 2023;
in revised form August 31, 2023;
accepted September 28, 2023